Korean Journal of Radiology

KJR

Development and Validation of ^{18}F-FDG PET/CT-Based Multivariable Clinical Prediction Models for the Identification of Malignancy-Associated Hemophagocytic Lymphohistiocytosis

Xu Yang[1]*, Xia Lu[1]*, Jun Liu[1], Ying Kan[1], Wei Wang[1], Shuxin Zhang[1], Lei Liu[2], Jixia Li[3, 4], Jigang Yang[1]

[1]Department of Nuclear Medicine, Beijing Friendship Hospital, Capital Medical University, Beijing, China; [2]Sinounion Medical Technology (Beijing) Co., Ltd., Beijing, China; [3]Department of Laboratory Medicine, School of Medicine, Foshan University, Foshan, China; [4]Department of Molecular Medicine and Pathology, School of Medical Science, The University of Auckland, Auckland, New Zealand

Objective: ^{18}F-fluorodeoxyglucose (FDG) PET/CT is often used for detecting malignancy in patients with newly diagnosed hemophagocytic lymphohistiocytosis (HLH), with acceptable sensitivity but relatively low specificity. The aim of this study was to improve the diagnostic ability of ^{18}F-FDG PET/CT in identifying malignancy in patients with HLH by combining ^{18}F-FDG PET/CT and clinical parameters.

Materials and Methods: Ninety-seven patients (age ≥ 14 years) with secondary HLH were retrospectively reviewed and divided into the derivation (n = 71) and validation (n = 26) cohorts according to admission time. In the derivation cohort, 22 patients had malignancy-associated HLH (M-HLH) and 49 patients had non-malignancy-associated HLH (NM-HLH). Data on pretreatment ^{18}F-FDG PET/CT and laboratory results were collected. The variables were analyzed using the Mann-Whitney U test or Pearson's chi-square test, and a nomogram for predicting M-HLH was constructed using multivariable binary logistic regression. The predictors were also ranked using decision-tree analysis. The nomogram and decision tree were validated in the validation cohort (10 patients with M-HLH and 16 patients with NM-HLH).

Results: The ratio of the maximal standardized uptake value (SUVmax) of the lymph nodes to that of the mediastinum, the ratio of the SUVmax of bone lesions or bone marrow to that of the mediastinum, and age were selected for constructing the model. The nomogram showed good performance in predicting M-HLH in the validation cohort, with an area under the receiver operating characteristic curve of 0.875 (95% confidence interval, 0.686–0.971). At an appropriate cutoff value, the sensitivity and specificity for identifying M-HLH were 90% (9/10) and 68.8% (11/16), respectively. The decision tree integrating the same variables showed 70% (7/10) sensitivity and 93.8% (15/16) specificity for identifying M-HLH. In comparison, visual analysis of ^{18}F-FDG PET/CT images demonstrated 100% (10/10) sensitivity and 12.5% (2/16) specificity.

Conclusion: ^{18}F-FDG PET/CT may be a practical technique for identifying M-HLH. The model constructed using ^{18}F-FDG PET/CT features and age was able to detect malignancy with better accuracy than visual analysis of ^{18}F-FDG PET/CT images.

Keywords: *Hemophagocytic lymphohistiocytosis; Malignancy; PET-CT; Diagnosis*

INTRODUCTION

Hemophagocytic lymphohistiocytosis (HLH) is a rare but life-threatening hyperinflammatory syndrome characterized by persistent activation of cytotoxic T cells, natural killer (NK) cells, and macrophages [1]. Primary HLH is generally caused by genetic mutations or familial inheritance, with an incidence of 1 in 50000–100000 live births [2]. In contrast, secondary HLH occurs in older children and adults. Currently, the precise incidence of HLH in adults is unknown, and the annual incidence is estimated to be approximately 1 in 800000 [3]. Various triggers have been linked to secondary HLH, including malignancy, infection, autoimmune disease, metabolic disease, and acquired immune deficiency. Secondary HLH can be categorized into two main types: malignancy-associated HLH (M-HLH) and non-malignancy-associated HLH (NM-HLH). Emerging data show that M-HLH accounts for approximately 40%–70% of secondary HLH in adults and has a worse prognosis, with a mortality rate of > 80% and a median survival time of < 2.0 months [2,4]. The vast majority of M-HLH cases are triggered by hematologic malignancies, including lymphomas, acute leukemia, lymphoproliferative diseases, and myelodysplastic syndrome [2]. The diagnosis of M-HLH is a challenge to clinicians owing to variable overlapping symptoms with other types of HLH, sepsis, and multiorgan failure, leading to high rates of misdiagnosis and poor outcomes. Treatment must be tailored to the identified trigger, patient performance, organ functions, and concomitant therapies. Prompt identification of the underlying trigger is essential to initiate appropriate therapy and reduce relapse in patients with M-HLH.

As mentioned above, accurate identification of malignancy in the context of HLH is extremely difficult. Bone marrow assessment is performed in all patients with HLH; however, a negative result does not exclude malignancy. Additionally, as the immune system is unable to adequately restrict the stimulatory effects of various triggers, the values of laboratory parameters may be affected in patients with M-HLH [4-8]. For example, increases in lactate dehydrogenase levels, beta-2-microglobulin levels, and soluble CD25 (sCD25)/ferritin ratio have been reported in M-HLH [5-7], whereas the fibrinogen levels and platelet count may be decreased [4,6]. A few studies have indicated that ^{18}F-fluorodeoxyglucose (FDG) PET/CT helps in detecting malignancy and guiding biopsy [9-12]; however, the imaging findings are not specific for HLH. In general,

^{18}F-FDG PET/CT shows hepatosplenomegaly and diffusely increased FDG uptake in the liver, spleen, axial skeleton, and multiple lymph nodes. These findings are partially due to the hyperinflammatory state in HLH and have a high false-positive rate in detecting malignancy. Our previous study highlighted that ^{18}F-FDG PET/CT alone is insufficient to make an accurate differential diagnosis, although it may help identify the potential trigger for secondary HLH [10]. Therefore, efforts focusing on the development of a novel strategy for the rapid and accurate identification of M-HLH are underway. This study was designed to evaluate the diagnostic performance of ^{18}F-FDG PET/CT in patients with secondary HLH with suspected malignancy and to develop novel predictive models for identifying M-HLH by combining PET/CT variables with clinical variables.

MATERIALS AND METHODS

Patients

This retrospective study was approved by the Institutional Review Board of Beijing Friendship Hospital of Capital Medical University, and the requirement for written informed consent was waived (IRB No. 2018-P2-006-01). The records of patients with HLH who underwent ^{18}F-FDG PET/CT between August 2016 and April 2021 at our department were retrospectively reviewed. All patients underwent pathology tests, and the diagnostic criteria for HLH and hematologic malignancy were in accordance with the HLH-2004 protocol [13] and the 2016 World Health Organization criteria [14]. Patients aged < 14 years or treated with chemotherapy or granulocyte colony-stimulating factor before ^{18}F-FDG PET/CT were excluded. Consecutive patients from August 2016 to June 2020 were enrolled in the derivation cohort, and consecutive patients from July 2020 to April 2021 were enrolled in the validation cohort. Consequently, 71 patients in the derivation cohort and 26 patients in the validation cohort were included in this study. On the basis of the physician's assessment or evidence from medical records, the patients in each cohort were divided into the M-HLH and NM-HLH groups (Fig. 1).

Clinical Data Collection

A standard form was used to record clinical parameters such as age, sex, and laboratory features (Tables 1-3). Data on laboratory features were collected before the initial HLH-specific therapy and within 7 days before or after ^{18}F-FDG PET/CT.
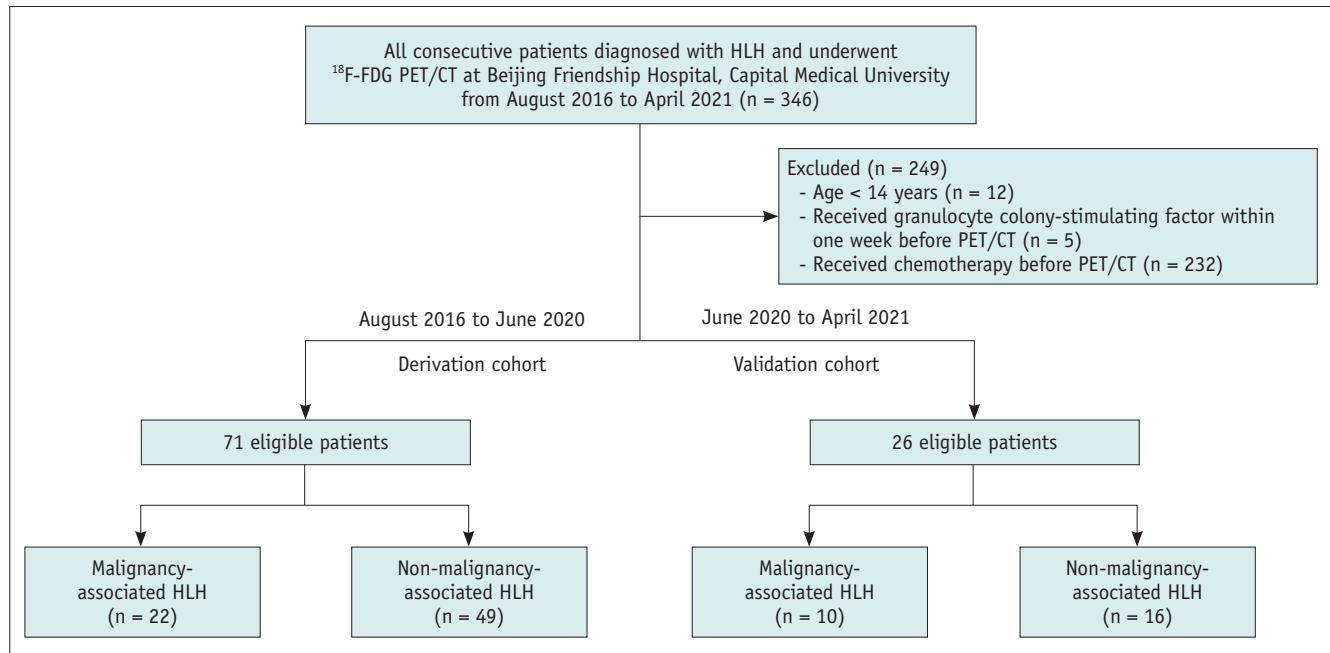
Fig. 1. Flowchart of patient enrollment. FDG = fluorodeoxyglucose, HLH = hemophagocytic lymphohistiocytosis

Table 1. Patients Characteristics

Characteristic	Derivation Cohort (n = 71)	Validation Cohort (n = 26)	P
Sex			0.603
Female	34 (47.9)	14 (53.8)	
Male	37 (52.1)	12 (46.2)	
Age at the time of HLH diagnosis, years			0.149
Median	38	48	
Range	14–79	16–76	
Malignancy associated HLH	22 (31.0)	10 (38.5)	0.626
B cell neoplasms	11 (50.0)	4 (40.0)	
Diffuse large B-cell lymphoma	6 (54.5)	3 (75.0)	
Classical Hodgkin lymphoma	2 (18.2)		
Non-Hodgkin B cell lymphoma	1 (9.1)		
Follicular lymphoma	1 (9.1)	1 (25.0)	
B-cell acute lymphocytic leukemia	1 (9.1)		
T/NK cell neoplasms	11 (50)	5 (50.0)	
NK/T-cell lymphoma	6 (54.5)	2 (40.0)	
T-cell lymphoma	2 (18.2)		
Peripheral T-cell lymphoma	2 (18.2)	2 (40.0)	
Anaplastic large cell lymphoma	1 (9.1)		
Angioimmunoblastic T-cell lymphoma		1 (20.0)	
Myelodysplastic/myeloproliferative neoplasm		1 (10.0)	
Non-malignancy associated HLH	49 (69.0)	16 (61.5)	0.884
EBV infection	24 (49.0)	6 (37.5)	
Other infections	12 (24.5)	4 (25.0)	
Adult Still's disease	5 (10.2)	2 (12.5)	
Systemic lupus erythematosus	1 (2.0)	1 (6.25)	
Undifferentiated systemic rheumatic disease	1 (2.0)		
Unknown	6 (12.2)	3 (18.8)	

Data are number of patients with percentage in parentheses, unless specified otherwise. EBV = Epstein–Barr virus, HLH = hemophagocytic lymphohistiocytosis, NK = natural killer

Table 2. The Comparison of Baseline ^{18}F-FDG PET/CT Findings in the Derivation Cohort

Variables	M-HLH (n = 22)	NM-HLH (n = 49)	P
Clinical variables			
Male	16 (72.7)	21 (42.9)	0.020*
Age, year	49 (32–58)	33 (25–52)	0.041*
Lymph node features			
High FDG uptake	17 (77.3)	28 (57.1)	0.103
Long diameter	1.8 (1.1–2.4)	1.6 (1.3–2.0)	0.851
Short diameter	1.3 (0.8–1.7)	1.0 (0.7–1.3)	0.313
SUVmax-lymph nodes	12.9 (3.7–19.7)	4.6 (3.5–9.7)	0.022*
SUVmax-lymph nodes/mediastinum	10.2 (2.8–14.5)	3.1 (2.3–6.1)	0.013*
Asymmetry	14 (82.4)	10 (35.7)	0.002*
Bone features			
Focal bone lesion	15 (68.2)	8 (16.3)	< 0.001*
SUVmax-bone lesions or bone marrow	7.6 (4.9–17.1)	4.1 (3.7–5.3)	< 0.001*
SUVmax-bone lesions or bone marrow/mediastinum	4.9 (2.6–14.4)	2.7 (2.2–3.4)	< 0.001*
Spleen features[†]			
Focal spleen lesion	7 (33.3)	6 (12.2)	0.081
SUVmax-spleen	4.2 (3.1–9.6)	3.2 (2.4–4.4)	0.009*
SUVmax-spleen/mediastinum	2.0 (1.8–7.7)	1.8 (1.5–2.8)	0.001*
Volume-spleen	650 (516–1038)	432 (281–878)	0.008*
TLG-spleen	1791 (1212–2598)	961 (463–1688)	0.003*
Liver features			
Focal liver lesion	5 (22.7)	1 (2.0)	0.015*
SUVmax-liver	3.9 (3.1–8.6)	2.9 (2.5–3.4)	0.001*
SUVmax-liver/mediastinum	2.3 (1.7–8.3)	1.8 (1.7–2.2)	< 0.001*
Volume-liver	1980 (1525–2479)	1549 (1212–1966)	0.020*
TLG-liver	4171 (3042–5628)	3089 (2179–3896)	0.001*

Data are median (interquartile range) or number of patients (percentage). *Significance at $p < 0.05$, [†]One HLH patient with hematologic malignancy had been removed spleen, so the number of M-HLH spleen features is 21. FDG = fluorodeoxyglucose, HLH = hemophagocytic lymphohistiocytosis, M-HLH = malignancy-associated HLH, NM-HLH = non-malignancy-associated HLH, SUVmax = maximal standardized uptake value, TLG = total lesion glycolysis

^{18}F-FDG PET/CT Image Acquisition and Analysis

All ^{18}F-FDG PET/CT images were acquired using a Siemens Biograph mCT PET/CT scanner (Siemens). The patients were instructed to fast for 6 hours, and the blood glucose levels were confirmed to be < 11.1 mmoL/L. Approximately 4.4 MBq/kg ^{18}F-FDG was intravenously injected before PET/CT. After a 60-minute uptake time, CT was first performed with the following parameters: 140 kV, automatic mA, and layer thickness of 3 mm. Thereafter, PET was performed with an acquisition time of 2.5 minutes per bed position in three-dimensional mode. PET images were reconstructed using the ordered subset expectation maximization iterative method with CT information for attenuation correction.

Two experienced nuclear medicine physicians with > 5 years' experience in PET/CT diagnosis reviewed the PET/CT images on a dedicated workstation (syngo MultiModality Workplace, Siemens). The presence of hypermetabolic lymph nodes and their distributions were recorded. The maximal standardized uptake value (SUVmax) of the lymph node with the highest FDG uptake and its short and long axes were documented. In the bone marrow, focal increased FDG uptake and the SUVmax of bone lesions were recorded. In the absence of focal hypermetabolic bone lesions, an ellipsoidal region of interest was drawn in lumbar vertebrae 4 to measure the SUVmax of the bone marrow. Hypermetabolic foci caused by other factors (e.g., bone marrow puncture or degeneration) were excluded. In the liver and spleen, focal increased FDG uptake, SUVmax, volume, and total lesion glycolysis (TLG) were documented. SUVmax, volume, and TLG were measured using 3D Slicer™ software (version 4.10.0, http://www.slicer.org). The TLG of the liver and spleen was calculated by multiplying the SUVmean by the total volume. As a reference value, the SUVmax of the mediastinum was measured by drawing

Table 3. The Comparison of Baseline Laboratory Oarameters in the Derivation Cohort

Variables	M-HLH (n = 22)		NM-HLH (n = 49)*		P
	n[†]	Summary Measure	n[†]	Summary Measure	
Laboratory parameters	22		47		
WBC, x 10⁹/L		2.56 (1.40–5.44)		4.90 (2.04–7.18)	0.076
ANC, x 10⁹/L		1.42 (0.76–3.01)		2.65 (1.20–4.97)	0.083
HGB, g/L		77.5 (66.8–110.0)		93.0 (84.0–104.0)	0.166
PLT, x 10⁹/L		67.5 (33–94)		107.0 (57–191)	0.035[§]
CRP, mg/L		47.4 (10.8–94.2)		15.0 (3.0–42.5)	0.011[§]
ALT, U/L		46.5 (19.5–105.5)		56.0 (32.0–100.0)	0.507
AST, U/L		68.5 (39.7–137.8)		62.9 (29.3–113.2)	0.421
TG, mmoL/L		2.04 (1.5–2.8)		1.89 (1.4–2.6)	0.532
SF, ng/mL	22	1957.2 (1226.8–5692.5)	46	1390.0 (440.3–3910.8)	0.132
FBG, g/L		2.84 (1.71–3.93)		2.01 (1.42–3.02)	0.155
ESR, mm/h	22	25.5 (10.0–57.5)	46	20 (10.0–36.5)	0.273
LDH, U/L		719 (464–1374)		455 (284–737)	0.028[§]
sCD25, pg/mL	20	39516 (9561–44000)	42	10038.5 (3589–29099)	0.004[‖]
sCD25/SF	20	10.2 (2.1–23.9)	42	5.9 (1.7–23.0)	0.598
β2-MG, mg/L	20	4.18 (3.20–4.96)	35	3.17 (2.30–4.82)	0.090
Inflammatory cytokines[‡], pg/mL	17		33		
IL-1α		0.40 (0.31–1.36)		0.40 (0.30–0.60)	0.732
IL-1β		1.00 (0.70–1.95)		1.20 (0.76–1.85)	0.735
IL-2		3.40 (2.50–4.10)		3.40 (2.50–5.70)	0.538
IL-4		5.60 (3.00–20.77)		5.31 (4.25–7.10)	0.984
IL-6		8.90 (4.45–42.85)		5.20 (4.05–22.80)	0.282
IL-8		12.00 (3.64–25.35)		1.40 (1.00–19.10)	0.025[§]
IL-10		45.70 (8.57–194.85)		1.40 (1.00–41.00)	0.007[‖]
IL-12		3.40 (2.75–5.50)		3.40 (2.60–6.15)	0.878
IL-17		1.10 (0.70–1.40)		0.90 (0.60–1.20)	0.340
IL-18		168.10 (75.39–390.98)		262.80 (49.61–533.75)	0.862
IL-23		8.10 (4.81–11.70)		6.70 (4.45–8.63)	0.384
IFN-α		0.20 (0.15–0.28)		0.20 (0.19–0.30)	0.272
IFN-γ		190.40 (67.25–265.42)		125.70 (28.35–676.90)	0.975
GM-CSF		7.00 (5.95–7.15)		6.90 (5.14–8.10)	0.984
TNF-α		10.70 (4.60–25.75)		13.40 (5.40–31.85)	0.798
EBV infection	22	11 (50)	49	24 (49)	0.937
Hemophagocytosis	22	16 (72.7)	48	32 (66.7)	0.612

Data are median (interquartile range) or number of patients (percentage). *The number of NH-HLH group is 47 because 2 HLH patients lacked available laboratory data, [†]Data are number of patients with data available, blank indicates no missing data, [‡]The number of patients whose cytokines is available is 17 and 33 with M-HLH and NM-HLH respectively, [§]Significance at $p < 0.05$, [‖]Significance at $p < 0.01$. ALT = alanine aminotransferase, ANC = absolute neutrophil count, AST = aspartate aminotransferase, CRP = C-reactive protein, ESR = erythrocyte sedimentation rate, FBG = fibrinogen, GM-CSF = granulocyte-macrophage colony stimulating factor, HGB = hemoglobin, HLH = hemophagocytic lymphohistiocytosis, IFN = interferon, IL = interleukin, LDH = lactate dehydrogenase, M-HLH = malignancy-associated HLH, NM-HLH = non-malignancy-associated HLH, PLT = platelet count, sCD25 = soluble interleukin-2 receptor (sIL-2R), SF = serum ferritin, TG = triglycerides, TNF = tumor necrosis factor, WBC = white blood cell, β2-MG = beta-2-microglobulin

a 1-cm-diameter sphere in the aortic arch. The ratios were calculated as the SUVmax of the lymph nodes, bone marrow, liver, and spleen divided by the SUVmax of the mediastinum.

Statistical Analysis

Statistical analyses were performed using SPSS statistical software (version 26.0, IBM Corp.), MedCalc statistical software (version 19.0.7, MedCalc Software bvba), and R (version 4.0.3, http://www.r-project.org). Continuous variables are presented as medians with interquartile ranges. Categorical variables are presented as frequencies and percentages. Skewed continuous variables were compared using the Mann-Whitney U test, and categorical variables

PET/CT-Based Models for Identifying Malignancy-Associated HLH

Korean Journal of Radiology
KJR

were compared using Pearson's chi-square (χ^2) or Fisher's exact test. All *p* values were two-sided, with significance set at *p* < 0.05. Multivariable logistic regression with a stepwise approach was performed to select independent predictors. Predictive models were constructed using logistic equations and simplified into a nomogram. Collinearity diagnostic analyses were performed. Calibration curves were plotted to improve the prediction accuracy of the nomogram. The selected predictors were used in decision-tree analysis, which quantifies information gain. The diagnostic ability of the variables and predictive models were determined using receiver-operating characteristic curve analysis, and cutoff values were estimated. Decision curve analysis was used to assess the clinical usefulness of the models. Finally, we applied our predictive models to the validation cohort for verification.

RESULTS

Characteristics of Patients

The characteristics of 71 patients in the derivation cohort and 26 patients in the validation cohort are shown in Table 1. No statistical differences in sex (*p* = 0.603), age (*p* = 0.149), and triggers of M-HLH (*p* = 0.626) and NM-HLH (*p* = 0.884) were found between the two cohorts. M-HLH was diagnosed in 22 (31.0%) patients in the derivation cohort and in 10 (38.5%) patients in the validation cohort. The percentages of B-cell neoplasms and T/NK cell neoplasms were similar between the two cohorts. In both cohorts, the most frequent cause of M-HLH was diffuse

large B-cell lymphoma and the most common trigger of NM-HLH was Epstein-Barr virus (EBV) infection.

Comparison of Baseline ^{18}F-FDG PET/CT Findings and Laboratory Data between M-HLH and NM-HLH in the Derivation Cohort

The ^{18}F-FDG PET/CT variables and laboratory features are compared in Tables 2 and 3. In terms of sex and age, M-HLH seemed to be more common in male and older patients. The percentage of male patients was higher and age was older in the M-HLH group than in the NM-HLH group (*p* = 0.020 and *p* = 0.041). Most PET/CT variables were significantly different between the two groups. For instance, asymmetrical distribution of hypermetabolic lymph nodes (*p* = 0.002), bone lesions (*p* < 0.001), and focal liver lesions (*p* = 0.015) were more frequently observed in the M-HLH group. Moreover, patients with M-HLH tended to have higher SUVmax of the lymph nodes and bone lesions, as well as higher SUVmax, volume, and TLG of the spleen and liver than patients with NM-HLH (*p* < 0.05). No differences between the groups were observed in terms of hypermetabolic lymph nodes and long and short diameters of the lymph node with the highest FDG uptake. With respect to laboratory parameters, the white blood cell, absolute neutrophil, and platelet counts were lower, whereas the C-reactive protein, lactate dehydrogenase, sCD25, beta-2-microglobulin, interleukin (IL)-8, and IL-10 levels were higher in patients with M-HLH than in those with NM-HLH (*p* < 0.05).
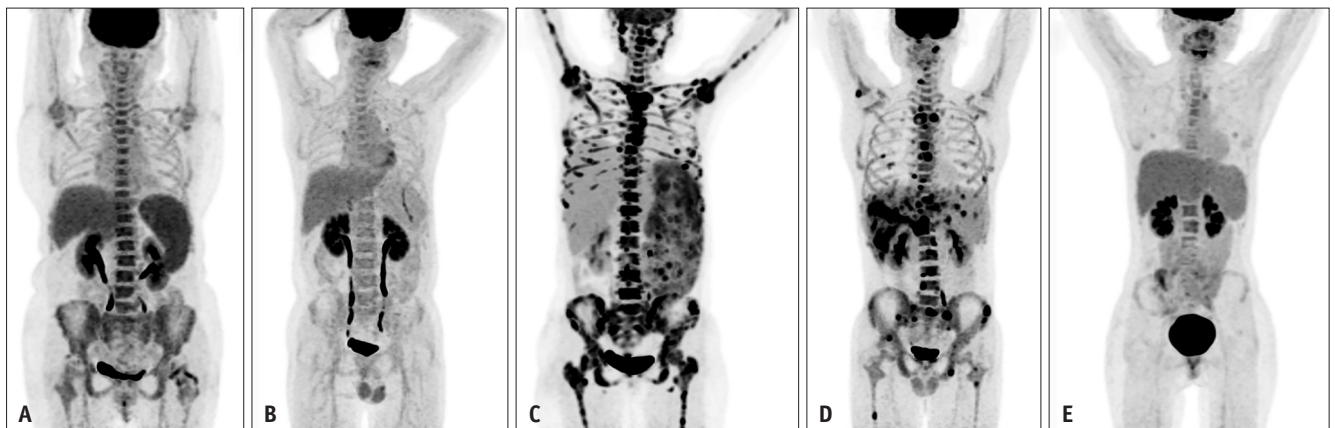
Fig. 2. False-negative and false-positive ^{18}F-FDG PET/CT maximum intensity projection images in patients with HLH.
A-E. A 66-year-old female diagnosed with non-Hodgkin B-cell lymphoma based on bone marrow biopsy **(A)** and a 56-year-old male diagnosed with T-cell lymphoma based on bone marrow biopsy **(B)** both showed no lesions with focal FDG uptake. A 23-year-old female diagnosed with chronic active EBV infection **(C)** and a 30-year-old male diagnosed with EBV-associated HLH **(D)** both showed multiple hypermetabolic foci mimicking a lymphoma. A 19-year-old female without malignancy showed patchy FDG uptake within the vertebrae and pelvis **(E)**. EBV = Epstein–Barr virus, FDG = fluorodeoxyglucose, HLH = hemophagocytic lymphohistiocytosis

Diagnostic Performance of Visual Analysis of ^{18}F-FDG PET/CT Images

Patients were considered positive for malignancy if the ^{18}F-FDG PET/CT images showed hypermetabolic lymph nodes or focal increased FDG uptake in the bone, liver, or spleen. This approach enabled the diagnosis of M-HLH with 90.9%

Table 4. Multivariable Logistic Regression Models for Prediction of Malignancy in Patients with HLH

Variables	OR (95% CI)	P
Laboratory model (n = 62)		
Age	1.53 (1.04–2.25)*	0.029
sCD25	1.41 (1.10–1.80)†	0.006
^{18}F-FDG PET/CT model (n = 71)		
Age	2.04 (1.26–3.30)*	0.004
SUVmax-lymph nodes/ mediastinum	1.31 (1.10–1.55)	0.002
SUVmax of bone lesions or bone marrow/mediastinum	1.29 (1.09–1.52)	0.003

*The OR is for every 10 years of age increase, †The OR is for every 6400 pg/mL sCD25 increase. CI = confidence interval, FDG = fluorodeoxyglucose, OR = Odds ratio, sCD25 = soluble interleukin-2 receptor (sIL-2R), SUVmax = maximal standardized uptake value

sensitivity (20/22), 36.7% specificity (18/49), and 53.5% accuracy in the derivation cohort. Similar to the derivation cohort, visual analysis showed 100% sensitivity (10/10), 12.5% specificity (2/16), and 46.2% accuracy in the validation cohort.

The false-negative PET/CT images of two patients with M-HLH in the derivation cohort are shown in Figure 2A and B. Notably, multifocal increased FDG uptake in the bone marrow was common in patients with EBV infection (positive predictive value for malignancy: 53.3%, 8/15) (Fig. 2C, D), but was a sign of malignancy in patients without EBV infection (positive predictive value: 87.5%, 7/8). Only one patient without malignancy and EBV infection had focal hypermetabolic bone lesions (Fig. 2E). This patient had cytomegalovirus infection, and the SUVmax of bone lesions was the lowest at 3.9. Focal spleen or liver lesions were observed in 15 patients, and the potential causes were malignancy (9/15), EBV infection (5/15), and unknown (1/15).
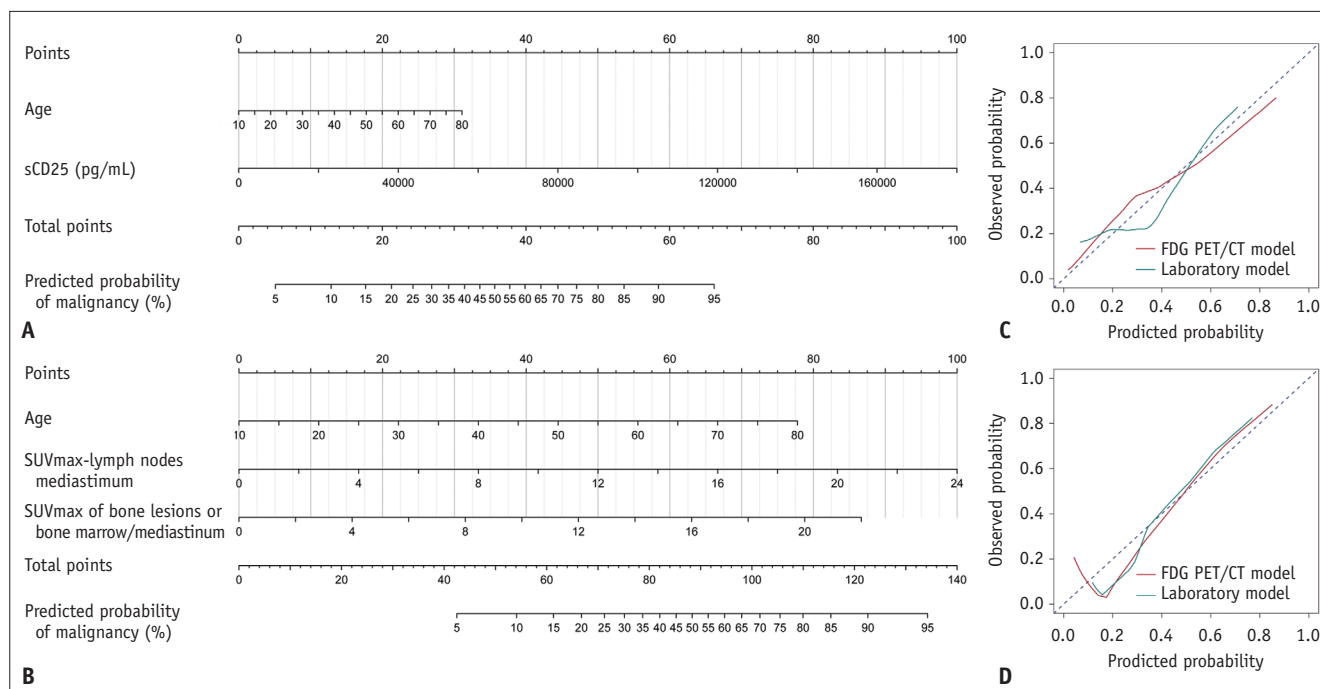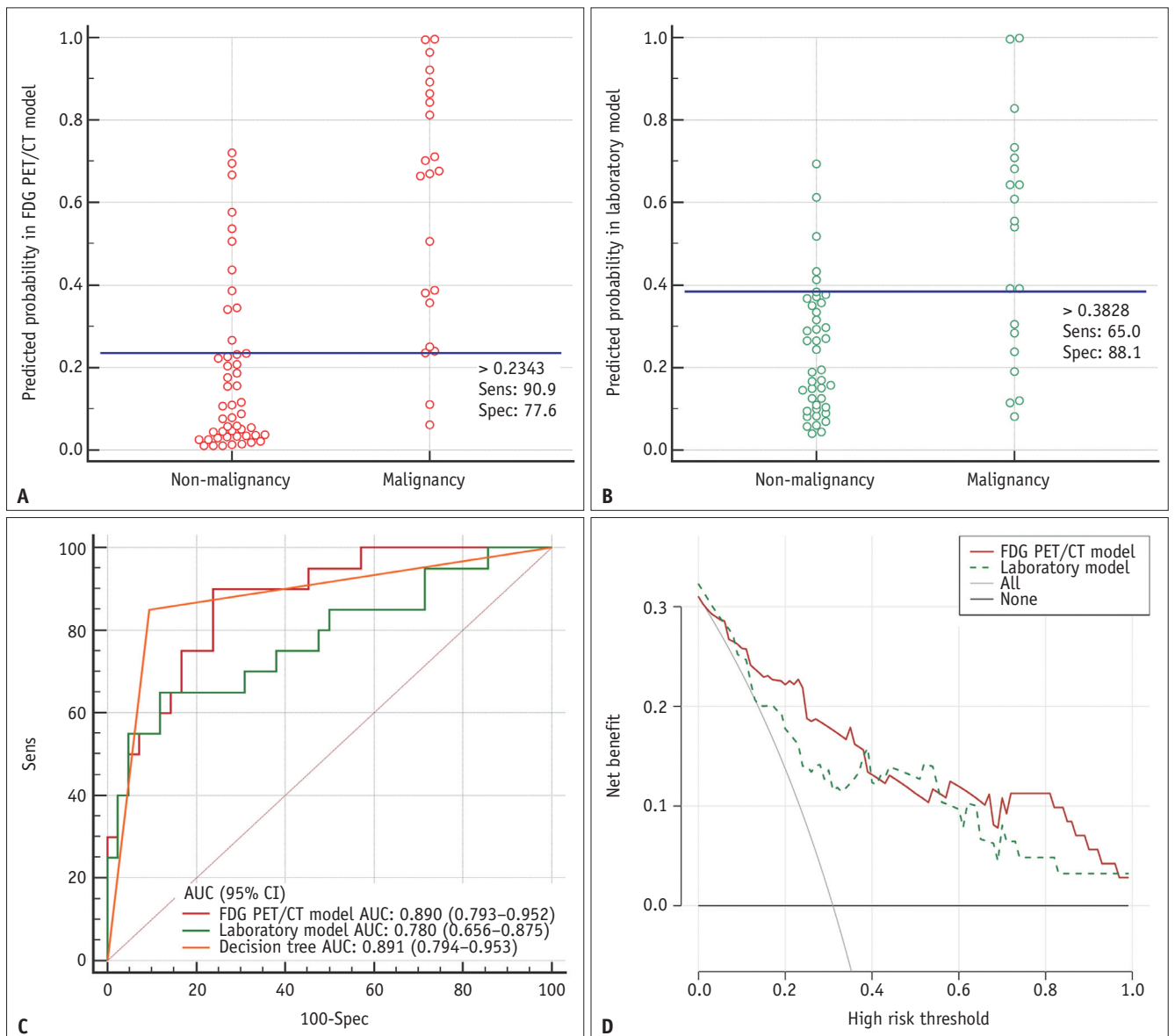

Fig. 3. Nomograms for predicting malignancy in patients with hemophagocytic lymphohistiocytosis (A, B) and their calibration curves in the derivation (C) and validation (D) cohorts. In nomogram **(A)**, points for age and sCD25 level can be obtained by calibrating with the point caliper. Thereafter, the points are combined to obtain a total score that can be calibrated with the predicted probability scale. In nomogram **(B)**, points for the lymph node/mediastinum SUVmax ratio and bone lesion or bone marrow/mediastinum SUVmax ratio can also be obtained by calibrating with the point caliper. Thereafter, the points are added to the total points to improve the prediction accuracy. The blue dotted lines on the diagonal are the reference lines indicating that the predicted value is equal to the actual value. The green and red lines are the calibration curves representing nomograms **(A)** and **(B)**, respectively. FDG = fluorodeoxyglucose, sCD25 = soluble interleukin-2 receptor (sIL-2R), SUVmax = maximal standardized uptake value

Table 5. Comparison of Performance of Models in Predicting Malignancy in Patients with Hemophagocytic Lymphohistiocytosis

Model	Derivation Cohort (n = 71)					Validation Cohort (n = 26)			
	Cutoff, %	Sensitivity, % (n = 22)	Specificity, % (n = 49)	Accuracy, % (n = 71)	AUC (95% CI)	Sensitivity, % (n = 10)	Specificity, % (n = 16)	Accuracy, % (n = 26)	AUC (95% CI)
Laboratory model	38.3	65.0 (n = 20)	88.1 (n = 42)	80.6 (n = 62)	0.780 (0.656–0.875)	77.8 (n = 9)	93.3 (n = 15)	87.5 (n = 24)	0.859 (0.657–0.966)
^{18}F-FDG PET/CT model	23.4	90.9	77.6	81.7	0.890 (0.793–0.952)	90.0	68.8	76.9	0.875 (0.686–0.971)
Decision tree	+	86.4	91.8	90.1	0.891 (0.794–0.953)	70.0	93.8	84.6	0.819 (0.619–0.941)

AUC = area under receiver operating characteristic curve, CI = confidence interval, FDG = fluorodeoxyglucose

Fig. 4. The evaluation of the models in the derivation cohort.
A, B. Interactive dot diagrams of the two multivariable logistic regression models for predicting malignancy in patients with hemophagocytic lymphohistiocytosis. **C.** Receiver operating characteristic curves of the two models, and the decision tree. **D.** Decision curve analysis for the above-mentioned models. The Y-axis represents the net benefit. AUC = area under the receiver operating characteristic curve, CI = confidence interval, FDG = fluorodeoxyglucose, Sens = sensitivity, Spec = specificity

Multivariable Logistic Regression Models

^{18}F-FDG PET/CT and laboratory parameters were analyzed separately and conjointly using multivariable logistic regression. The collinearity diagnostic analyses (Supplementary Table 1) did not indicate a significant collinearity between the variables in the models (tolerance > 0.2 and variance inflation factor < 5). Lastly, two PET/CT variables (lymph node/mediastinum SUVmax ratio and bone lesion or bone marrow/mediastinum SUVmax ratio) and two laboratory variables (age and sCD25 level) were selected to build the predictive models. The odds ratios and p values of these variables are shown in Table 4. The logistic models were used to construct nomograms. One nomogram was based on laboratory variables alone (laboratory model), and the other nomogram included PET/CT variables (^{18}F-FDG PET/CT model) (Fig. 3).

The diagnostic performance of each parameter is shown in Supplementary Table 2. Although none of the parameters were individually suited to predict malignancy, Table 5 shows interesting data. The laboratory model constructed using age and sCD25 level showed acceptable diagnostic accuracy with an area under the receiver operating characteristic curve (AUC) of 0.780 (95% confidence interval, 0.656–0.875) (Fig. 4B, C). At a cutoff value of 38.3%, the sensitivity and specificity of the model were 65.0% and 88.1%, respectively. Remarkably, the ^{18}F-FDG PET/CT model built using the lymph node/mediastinum SUVmax ratio, bone lesion or bone marrow/mediastinum SUVmax ratio, and age had a higher AUC (0.890; 95% confidence interval, 0.793–0.952) (Fig. 4A, C). At a cutoff value of 23.4%, the sensitivity and specificity of the model were 90.9% and 77.6%, respectively. The decision curve analysis showed that the ^{18}F-FDG PET/CT model had greater clinical utility for the prediction of malignancy than models established using laboratory variables alone (Fig. 4D).

Decision Tree for Diagnosing M-HLH

The decision tree predicted malignancy with a sensitivity of 86.4% (19/22), a specificity of 91.8% (45/49), and an accuracy of 90.1% (64/71) (Fig. 5, Table 5). M-HLH was identified in 90.0% (9/10) of patients with lymph node/mediastinum SUVmax ratio ≥ 10.0 and in 76.9% (10/13) of patients with lymph node/mediastinum SUVmax ratio < 10.0, focal bone lesions, and age ≥ 31 years.

Validation of the Models in the Validation Cohort

We applied our two logistic models and the decision tree
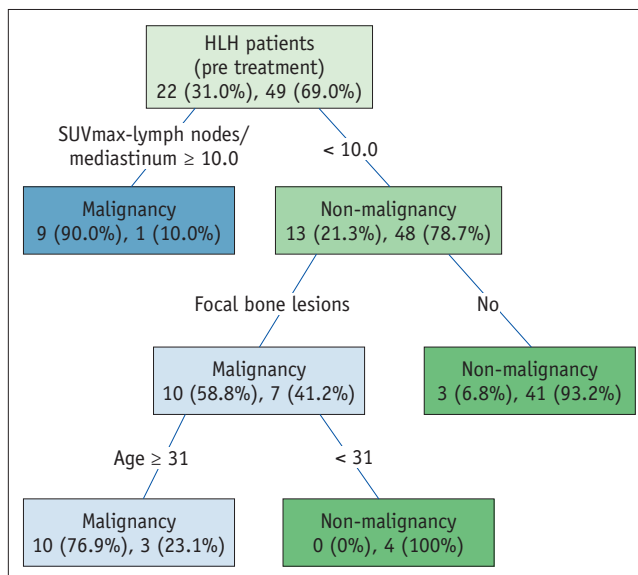
Fig. 5. A model for predicting malignancy in patients with HLH based on decision-tree analysis in the derivation cohort. HLH = hemophagocytic lymphohistiocytosis, SUVmax = maximal standardized uptake value

to the validation cohort (Table 5). Figure 6 shows that the models were well validated and had an acceptable discrimination ability (AUC > 0.8). The ^{18}F-FDG PET/CT model exhibited the best predictive performance in the validation cohort, with a classification accuracy, sensitivity, and specificity of 76.9%, 90.0%, and 68.8%, respectively.

DISCUSSION

In recent years, ^{18}F-FDG PET/CT has been suggested as a method for detecting potential triggers for secondary HLH [15,16]. Because of cytokine storm, reticuloendothelial system activation, and myeloproliferation, ^{18}F-FDG PET/CT images nonspecifically show diffusely increased FDG uptake in the liver, spleen, and axial skeleton [17-19]. Hence, it is necessary to improve the diagnostic specificity of ^{18}F-FDG PET/CT for prompt and precise detection of M-HLH. In the present study, ^{18}F-FDG PET/CT assisted in identifying malignancy in patients with secondary HLH, and a multivariable model combining ^{18}F-FDG PET/CT and clinical variables was established to predict malignancy before treatment. The decision tree showed an ability to conveniently predict M-HLH with acceptable diagnostic accuracy.

Visual analysis of ^{18}F-FDG PET/CT images has shown a high sensitivity but a relatively low specificity for malignancy detection in HLH. One study with a small
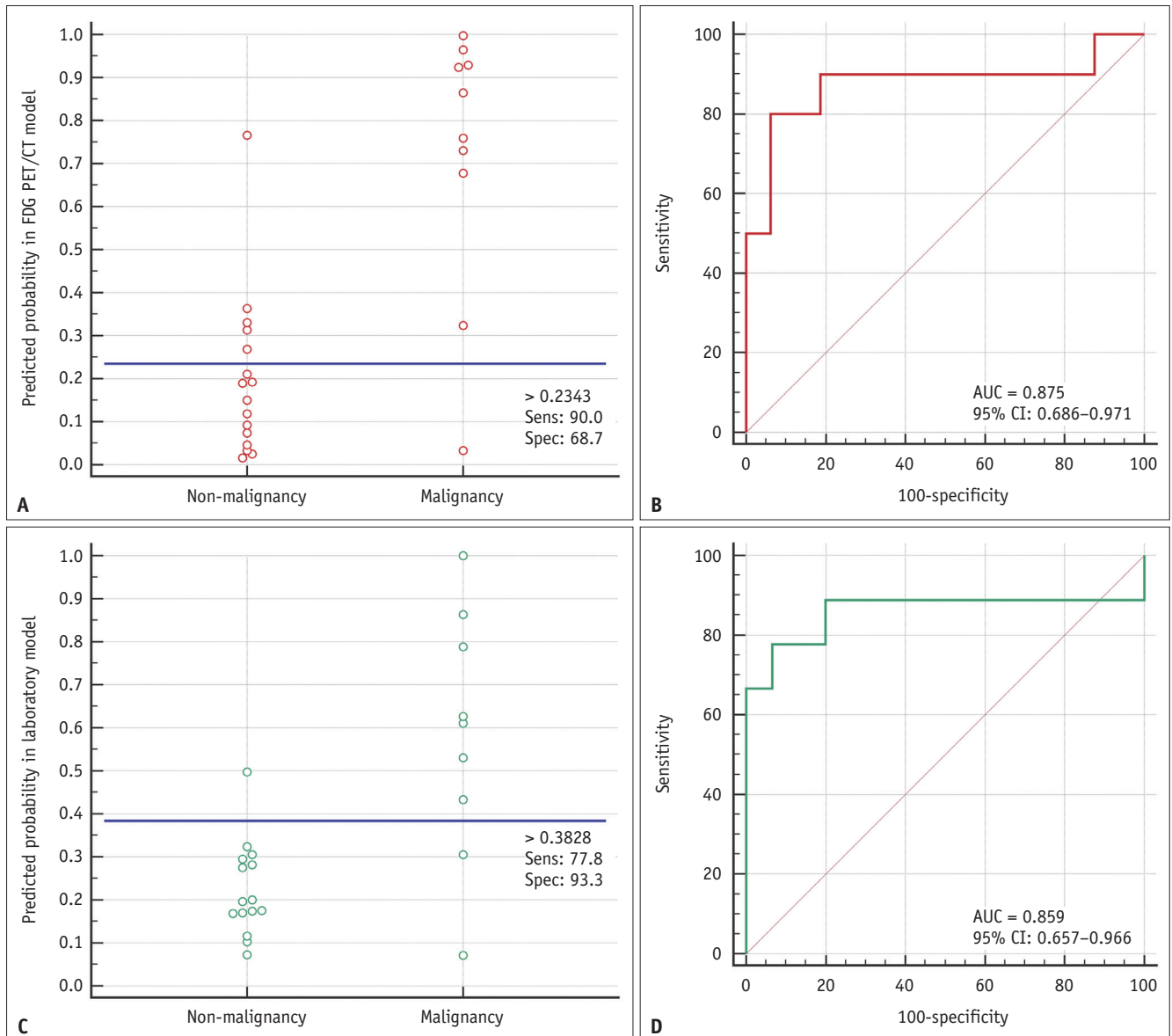
Fig. 6. Interactive dot diagrams (A, C) and receiver operating characteristic curves (B, D) of the two logistic models for differentiating malignancy-associated from non-malignancy-associated hemophagocytic lymphohistiocytosis in the validation cohort. The cutoff values used in the validation cohort were the same as those used in the derivation cohort. AUC = area under the receiver operating characteristic curve, CI = confidence interval, FDG = fluorodeoxyglucose, Sens = sensitivity, Spec = specificity

sample size (n = 14) reported that the sensitivity and specificity of ^{18}F-FDG PET/CT for detecting M-HLH were 83.0% and 62.5%, respectively [12]. In addition, several studies suggested that focal FDG uptake was a predictive sign of an underlying malignancy [9,11,20]. However, some studies found that the extranodal NK/T-cell lymphoma nasal type, aggressive NK cell leukemia, and some types of B-cell lymphoma occasionally lack lesions with focal FDG uptake [9,12,19]. Multiple hypermetabolic lymph nodes or patchy bone lesions were observed in several cases of EBV-associated HLH [12,21-23]. In the absence of

EBV infection, lesions with focal FDG uptake in the bone marrow are a reliable sign of malignancy in secondary HLH. Although multiple lymphadenopathies with increased FDG uptake more frequently occur in lymphoma-associated HLH than in non-lymphoma-associated HLH [11], infections and autoimmune diseases are often associated with hypermetabolic lymph nodes. Our data suggested that an asymmetrical distribution of hypermetabolic lymph nodes may suggest malignancy. Furthermore, our results indicated that both focal splenic FDG uptake and focal hepatic FDG uptake were closely linked to EBV infection and cannot

indicate malignancy. Additionally, patients with M-HLH had higher values of bone lesion, lymph node, spleen, and liver SUVmax than those with NM-HLH, consistent with previous reports [11,24]; however, no studies have reported about the volume and TLG of the liver and spleen thus far. The present study showed that the volume and TLG of the liver and spleen in the M-HLH group were higher than those in the NM-HLH group.

In addition to PET/CT variables, laboratory variables can help differentiate M-HLH from NM-HLH. Previous studies have shown that patients with lymphoma-associated HLH have lower fibrinogen levels and platelet count or higher lactate dehydrogenase and beta-2-microglobulin levels than patients with NM-HLH [4,6,7]. C-reactive protein plays both pro- and anti-inflammatory roles as a prototypical acute-phase serum protein [25], and its level is elevated in many malignancies [26]. Importantly, C-reactive protein serves as a good indicator of the usefulness of ^{18}F-FDG PET/CT in HLH [9]. Cytokine profiles vary in HLH with different underlying etiologies [27,28]. The interferon-γ and IL-10 levels are markedly elevated in HLH compared with sepsis [29], whereas the IL-18 level is starkly increased in macrophage activation syndrome [30]. The soluble IL-2 receptor, also known as the sCD25, is a T-cell activation marker. Its levels can be elevated in lymphoma, and a high sCD25/ferritin ratio has been reported to be a useful indicator of lymphoma-associated HLH [31]. The sCD25 level was a significant variable in our laboratory model; however, the sCD25/ferritin ratio was not significantly different between the two groups. This may be because of the difference in the patient sample.

In this study, a PET/CT-based multivariable model for malignancy was developed to improve the diagnostic ability of PET/CT. It is reasonable to infer that a high FDG uptake in focal bone lesions or bone marrow likely suggests skeletal involvement of malignancies, and a high FDG uptake in lymph nodes is likely due to lymphoma rather than reactive lymphoid hyperplasia. Age was always a crucial factor in diagnosing M-HLH in our study. Even in adults, younger age is associated with underlying genetic defects and is regularly accompanied by EBV infection [16].

A decision tree was executed to establish a model that is easy to use in the clinical setting. First, if a lymph node/mediastinum SUVmax ratio of ≥ 10.0 was observed, the patient very likely had M-HLH. When the lymph node/mediastinum SUVmax ratio was < 10.0, focal bone lesions and age were considered. When focal bone lesions were

present and age was ≥ 31 years, the possibility of M-HLH was very high. This model was simple and intuitive, with a predictive accuracy of 90.1% and 84.6% in the derivation and validation cohorts, respectively. However, the sensitivity of the decision tree was relatively lower than that of the ^{18}F-FDG PET/CT logistic regression model. Owing to the relatively low metabolic activity of a few types of lymphoma [32] and the absence of focal hypermetabolic bone lesions [19], false negatives cannot be avoided. Hence, biopsy of the bone marrow and lymph nodes was needed to confirm the diagnosis.

Our study had limitations. The small sample size, single-center design, and sample selection bias may affect the generalizability of the results. Occult malignancies may be difficult to detect and require repetitive tissue sampling. Even after a meticulous evaluation, undetectable malignancies may still be present in HLH. Heterogeneity among the patients was observed in terms of age, physical condition, and economic status. The predictive models should be further validated in prospective large multicenter cohorts.

In conclusion, ^{18}F-FDG PET/CT may be a practical technique for identifying M-HLH, and the nomogram constructed using ^{18}F-FDG PET/CT features and age was able to predict malignancy with better accuracy than visual analysis of PET/CT images. Future efforts should be made to further validate its diagnostic value in prospective large multicenter cohorts.

Supplement

The Supplement is available with this article at https://doi.org/10.3348/kjr.2021.0733.

Availability of Data and Material

The datasets generated or analyzed during the study are available from the corresponding author on reasonable request.

Conflicts of Interest

The authors have no potential conflicts of interest to disclose.

Author Contributions

Conceptualization: Shuxin Zhang, Jigang Yang. Data curation: Shuxin Zhang, Jun Liu, Xia Lu. Formal analysis: Ying Kan. Funding acquisition: Jigang Yang. Investigation:

ORCID iDs
Xu Yang
    https://orcid.org/0000-0001-7488-963X
Xia Lu
    https://orcid.org/0000-0003-2574-2281
Jun Liu
    https://orcid.org/0000-0002-1907-8989
Ying Kan
    https://orcid.org/0000-0001-8115-6071
Wei Wang
    https://orcid.org/0000-0001-8990-5516
Shuxin Zhang
    https://orcid.org/0000-0002-6946-3746
Lei Liu
    https://orcid.org/0000-0001-8268-2348
Jixia Li
    https://orcid.org/0000-0003-2218-5563
Jigang Yang
    https://orcid.org/0000-0002-0538-7676

REFERENCES

1. Al-Samkari H, Berliner N. Hemophagocytic lymphohistiocytosis. *Annu Rev Pathol* 2018;13:27-49
2. Daver N, McClain K, Allen CE, Parikh SA, Otrock Z, Rojas-Hernandez C, et al. A consensus review on malignancy-associated hemophagocytic lymphohistiocytosis in adults. *Cancer* 2017;123:3229-3240
3. Ramos-Casals M, Brito-Zerón P, López-Guillermo A, Khamashta MA, Bosch X. Adult haemophagocytic syndrome. *Lancet* 2014;383:1503-1516
4. Parikh SA, Kapoor P, Letendre L, Kumar S, Wolanskyj AP. Prognostic factors and outcomes of adults with hemophagocytic lymphohistiocytosis. *Mayo Clin Proc* 2014;89:484-492
5. Tabata C, Tabata R. Possible prediction of underlying lymphoma by high sIL-2R/ferritin ratio in hemophagocytic syndrome. *Ann Hematol* 2012;91:63-71
6. Li F, Li P, Zhang R, Yang G, Ji D, Huang X, et al. Identification of clinical features of lymphoma-associated hemophagocytic syndrome (LAHS): an analysis of 69 patients with hemophagocytic syndrome from a single-center in central region of China. *Med Oncol* 2014;31:902
7. Jiang T, Ding X, Lu W. The prognostic significance of Beta2 microglobulin in patients with hemophagocytic lymphohistiocytosis. *Dis Markers* 2016;2016:1523959
8. Yoon SE, Eun Y, Huh K, Chung CR, Yoo IY, Cho J, et al. A comprehensive analysis of adult patients with secondary hemophagocytic lymphohistiocytosis: a prospective cohort study. *Ann Hematol* 2020;99:2095-2104
9. Zheng Y, Hu G, Liu Y, Ma Y, Dang Y, Li F, et al. The role of 18F-FDG PET/CT in the management of patients with secondary haemophagocytic lymphohistiocytosis. *Clin Radiol* 2016;71:1248-1254
10. Yuan L, Kan Y, Meeks JK, Ma D, Yang J. 18F-FDG PET/CT for identifying the potential causes and extent of secondary hemophagocytic lymphohistiocytosis. *Diagn Interv Radiol* 2016;22:471-475
11. Wang J, Wang D, Zhang Q, Duan L, Tian T, Zhang X, et al. The significance of pre-therapeutic F-18-FDG PET-CT in lymphoma-associated hemophagocytic lymphohistiocytosis when pathological evidence is unavailable. *J Cancer Res Clin Oncol* 2016;142:859-871
12. Kim J, Yoo SW, Kang SR, Bom HS, Song HC, Min JJ. Clinical implication of F-18 FDG PET/CT in patients with secondary hemophagocytic lymphohistiocytosis. *Ann Hematol* 2014;93:661-667
13. Henter JI, Horne A, Aricó M, Egeler RM, Filipovich AH, Imashuku S, et al. HLH-2004: diagnostic and therapeutic guidelines for hemophagocytic lymphohistiocytosis. *Pediatr Blood Cancer* 2007;48:124-131
14. Cazzola M. Introduction to a review series: the 2016 revision of the WHO classification of tumors of hematopoietic and lymphoid tissues. *Blood* 2016;127:2361-2364
15. Canna SW, Marsh RA. Pediatric hemophagocytic lymphohistiocytosis. *Blood* 2020;135:1332-1343
16. La Rosée P, Horne A, Hines M, von Bahr Greenwood T, Machowicz R, Berliner N, et al. Recommendations for the management of hemophagocytic lymphohistiocytosis in adults. *Blood* 2019;133:2465-2477
17. Boddu P, Oviedo SP, Rausch CR, Yam C, Daver N, Kantarjian H, et al. PET-CT in AML-related hemophagocytic lymphohistiocytosis. *Leuk Lymphoma* 2018;59:1486-1489
18. Shieh AC, Guler E, Smith DA, Tirumani SH, Beck RC, Ramaiya NH. Hemophagocytic lymphohistiocytosis: a primer for radiologists. *AJR Am J Roentgenol* 2020;214:W11-W19
19. Yang YQ, Ding CY, Xu J, Fan L, Wang L, Tian T, et al. Exploring the role of bone marrow increased FDG uptake on PET/CT in patients with lymphoma-associated hemophagocytic lymphohistiocytosis: a reflection of bone marrow involvement or cytokine storm? *Leuk Lymphoma* 2016;57:291-298

20. Merrill SA, Naik R, Streiff MB, Shanbhag S, Lanzkron S, Braunstein EM, et al. A prospective quality improvement initiative in adult hemophagocytic lymphohistiocytosis to improve testing and a framework to facilitate trigger identification and mitigate hemorrhage from retrospective analysis. *Medicine (Baltimore)* 2018;97:e11579

21. Hao R, Yang X, Liu Z, Yang J. EBV-associated T-cell lymphoproliferative disorders demonstrated on FDG PET/CT in a patient with hemophagocytic lymphohistiocytosis. *Clin Nucl Med* 2019;44:829-830

22. Pan Q, Luo Y, Wu H, Ma Y, Li F. Epstein-Barr virus-associated hemophagocytic lymphohistiocytosis mimicking lymphoma on FDG PET/CT. *Clin Nucl Med* 2018;43:125-127

23. Lu J, Fang Q, Ma C, Su F, Chen G, Huang M, et al. Atypical Epstein-Barr virus-associated hemophagocytic lymphohistiocytosis simulating lymphadenitis on 18F-FDG PET/CT and its differential diagnosis. *Hell J Nucl Med* 2017;20:254-257

24. Zhang LJ, Xu J, Liu P, Ding CY, Li JY, Qiu HX, et al. The significance of 18F-FDG PET/CT in secondary hemophagocytic lymphohistiocytosis. *J Hematol Oncol* 2012;5:40

25. Marnell L, Mold C, Du Clos TW. C-reactive protein: ligands, receptors and role in inflammation. *Clin Immunol* 2005;117:104-111

26. Deme D, Telekes A. Prognostic importance of plasma C-reactive protein (CRP) in oncology. *Orv Hetil* 2017;158:243-256

27. Chen Y, Wang Z, Luo Z, Zhao N, Yang S, Tang Y. Comparison of Th1/Th2 cytokine profiles between primary and secondary haemophagocytic lymphohistiocytosis. *Ital J Pediatr* 2016;42:50

28. Ohno T, Ueda Y, Nagai K, Takahashi T, Konaka Y, Takamatsu T, et al. The serum cytokine profiles of lymphoma-associated hemophagocytic syndrome: a comparative analysis of B-cell and T-cell/natural killer cell lymphomas. *Int J Hematol* 2003;77:286-294

29. Xu XJ, Tang YM, Song H, Yang SL, Xu WQ, Zhao N, et al. Diagnostic accuracy of a specific cytokine pattern in hemophagocytic lymphohistiocytosis in children. *J Pediatr* 2012;160:984-990.e1

30. Weiss ES, Girard-Guyonvarc'h C, Holzinger D, de Jesus AA, Tariq Z, Picarsic J, et al. Interleukin-18 diagnostically distinguishes and pathogenically promotes human and murine macrophage activation syndrome. *Blood* 2018;131:1442-1455

31. Tsuji T, Hirano T, Yamasaki H, Tsuji M, Tsuda H. A high sIL-2R/ferritin ratio is a useful marker for the diagnosis of lymphoma-associated hemophagocytic syndrome. *Ann Hematol* 2014;93:821-826

32. Cronin CG, Swords R, Truong MT, Viswanathan C, Rohren E, Giles FJ, et al. Clinical utility of PET/CT in lymphoma. *AJR Am J Roentgenol* 2010;194:W91-W103